Geochemistry Geophysics Geosystems G3
AN ELECTRONIC JOURNAL OF THE EARTH SCIENCES
Published by AGU and the Geochemical Society

Article
Volume 10, Number 4
30 April 2009
Q04S13, doi:10.1029/2008GC002317
ISSN: 1525-2027

Triggered seismicity associated with the 1990 Nicoya, Costa Rica, M_w = 7.0 earthquake

Susan L. Bilek
Earth and Environmental Science Department, New Mexico Institute of Mining and Technology, Socorro, New Mexico 87801, USA (sbilek@nmt.edu)

Candy E. Elliott
Earth and Environmental Science Department, New Mexico Institute of Mining and Technology, Socorro, New Mexico 87801, USA

Now at AMEC Geomatrix, Rancho Cordova, California 95670, USA

Carolina Lithgow Bertelloni
Department of Earth Sciences, University College London, Gower Street, London WC1E 6BT, UK

[1] The 25 March 1990 (M_w = 7.0) subduction megathrust earthquake that occurred offshore the Nicoya Peninsula, Costa Rica, produced a large number of aftershocks on the subduction plate interface as expected and preceded an unusual sequence of earthquakes 75 km inland that had two periods of significant increase, one at 60–90 days and one near 270 days, following the main shock. This inland sequence of events would not typically fall within the classification of aftershocks given their spatial and temporal distance, and we show here that this sequence was likely triggered by the 25 March main shock. We compute stress changes on representative faults within this inland region using both a simple half-space model as well as with a 2-D finite element model that incorporates variable rheologic properties. The half-space model predicts a minor increase in Coulomb stress changes and a large amount of unclamping in this region, likely enough to cause triggering on the inland right-lateral strike-slip faults. Models that include a viscoelastic response also indicate stress increases that may link to triggering, particularly related to the time delay. Earthquakes on the subduction zone thrust along Costa Rica should be considered in hazard assessments for the inland populated region as several sets of strike-slip faults have been mapped in the fore-arc region.

Components: 8194 words, 11 figures, 1 table.

Keywords: Costa Rica; subduction; earthquake; triggering.

Index Terms: 7240 Seismology: Subduction zones (1207, 1219, 1240); 7230 Seismology: Seismicity and tectonics (1207, 1217, 1240, 1242); 7223 Seismology: Earthquake interaction, forecasting, and prediction (1217, 1242); 8164 Tectonophysics: Stresses: crust and lithosphere; 8170 Tectonophysics: Subduction zone processes (1031, 3060, 3613, 8413).

Received 11 November 2008; **Revised** 4 March 2009; **Accepted** 17 March 2009; **Published** 30 April 2009.

Bilek, S. L., C. E. Elliott, and C. L. Bertelloni (2009), Triggered seismicity associated with the 1990 Nicoya, Costa Rica, M_w = 7.0 earthquake, *Geochem. Geophys. Geosyst.*, *10*, Q04S13, doi:10.1029/2008GC002317.

Theme: Central American Subduction System
Guest Editors: G. Alvarado, K. Hoernle, and E. Silver

1. Introduction

[2] Following an earthquake, aftershocks typically occur in the region of coseismic slip as the fault plane readjusts to the postslip conditions. However, static or dynamic stresses produced as a result of coseismic slip during the main shock can trigger earthquakes well beyond the typical aftershock zone, up to 1000s of km away [e.g., *Stein*, 1999; *Steacy et al.*, 2004; *Freed*, 2005; *Parsons*, 2005]. The extent of the static triggering is limited to a few fault lengths away from the main rupture as the stress changes attenuate with distance from the fault [*Cotton and Coutant*, 1997; *Freed*, 2005].

[3] This mode of earthquake triggering has been an area of intense research since the recognition that stress changes introduced from one seismic event could lead to rupture of an adjacent section of the fault, widely recognized in the Landers–Big Bear sequence in California in 1992 [e.g., *Hauksson et al.*, 1993; *King et al.*, 1994]. The Big Bear earthquake, approximately 30 km west of the Landers epicenter, was a result of a 2–3 bar stress increase induced from the Landers earthquake rupture 3 h earlier [*King et al.*, 1994]. Static stress triggering does not only produce increased seismicity over hours, but many aftershock sequences that go on for days to years are explained by this mechanism [e.g., *Reasenberg and Simpson*, 1992; *Hardebeck et al.*, 1998; *Toda et al.*, 1998; *Anderson and Johnson*, 1999; *Lin and Stein*, 2004]. The October 1999 M_w = 7.1 Hector Mine earthquake is believed to be related to stress increases in the Landers–Big Bear earthquakes [*Dreger and Kaverina*, 2000], although other factors may have also influenced this event.

[4] Dynamic triggering, the result of small displacements on faults close to failure that are produced by passing surface waves from other earthquakes, is another primary mechanism to influence both near- and far-field seismicity. Triggered events can be a part of a near-field aftershock sequence, or could be at some distance away from the large event, such as those triggered in the western U.S. as a result of passing surface waves from the 1992 Landers [e.g., *Hill et al.*, 1993] and 2002 Denali, Alaska earthquakes [e.g., *Gomberg et al.*, 2004]. Recent work suggests that dynamic triggering is in fact a very common process, with 12 of a set of 15 $M > 7.0$ earthquakes showing evidence of remote triggering within a few hours after the rupture [*Velasco et al.*, 2008]. The time scale for dynamic triggering appears to be short however, with triggering occurring in the minutes to hours following the main earthquake.

[5] There are other secondary mechanisms that arise because of the primary stress changes that can also lead to earthquake triggering. These are cases of earthquake triggering beyond a few fault lengths from the main shock, but at weeks to months afterward, much later than would be suggested by the passage of surface waves. *Parsons* [2005] discussed a model of "delayed dynamic triggering" in which passing surface waves cause physical changes to the fault that shortens the recurrence rate for events on that fault. Changes in hydrologic conditions may also be important for earthquake triggering, as there have been observations of groundwater level changes following large earthquakes [e.g., *Roeloffs et al.*, 2003; *Brodsky et al.*, 2003; *Brodsky and Prejean*, 2005]. Fluid pressures likely increase significantly in the near field shortly after the slip event, thus acting to decrease the normal stresses and affect seismicity. However, these fluid pressure transients decay over time, again modifying the stresses and seismicity [*Freed*, 2005].

[6] Another possibility for delayed seismicity changes is viscoelastic relaxation in the region around the large event leading to increased stresses and seismicity at some later time from the original event [e.g., *Freed and Lin*, 1998; *Pollitz and Sacks*, 2002; *Freed*, 2005]. In these cases, the higher-temperature lower crust and mantle deform elastically in response to the rapid coseismic slip, but will relax over time, thus transferring stress into the upper crust. This mechanism has been suggested for the 1999 Hector Mine earthquake to explain its 7 year delay following the 1992 Landers earthquake sequence [*Freed and Lin*, 1998].

[7] Here we focus on issues of earthquake triggering within the Costa Rica portion of the Cocos-Caribbean subduction plate boundary. In particular, we examine the 25 March 1990 M_w = 7.0 subduction zone earthquake offshore the southern end of the Nicoya Peninsula in the Nicoya Gulf region (Figure 1). The subduction megathrust event was not unusual for the region and produced a typical aftershock pattern. More unusual was a sequence of small magnitude earthquakes that began approximately 75 km away from the epicentral area and continued throughout 1990, with peaks of activity between 60 and 90 days and around 270 days after the main shock slip. *Protti et al.* [1995] suggested that this inland seismic activity was triggered by the 25 March event, but they did not quantify stress

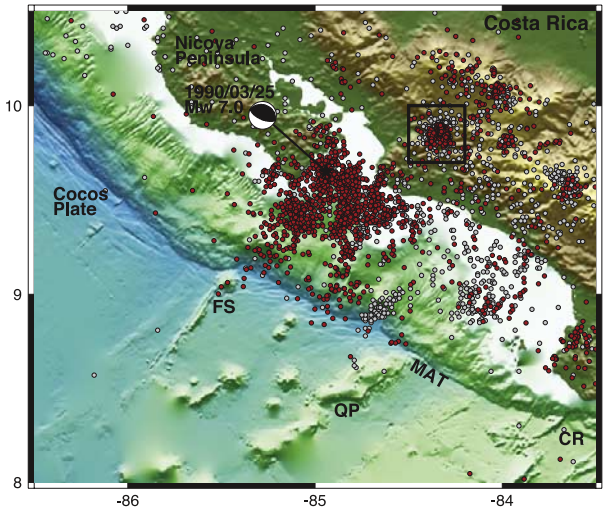

Figure 1. Map of western Costa Rica showing the location of the 25 March 1990 earthquake (star). Focal mechanism is from the inversion results of *Protti et al.* [1995]. Features on the subducting Cocos Plate include the Fisher Seamount Group (FS), the Quepos Plateau (QP), and the Cocos Ridge (CR). MAT is the Middle America Trench. Seismicity (red circles) includes all earthquakes with local magnitude >1.3 located by the OVSICORI seismic network (M. Protti and V. Gonzáles, personal communication, 2007) within the 90 days following the 25 March main shock. Gray circles show earthquakes through the remainder of 1990 (25 June to 31 December). Box highlights the inland region of seismicity that peaked approximately 75 days after the main shock. Bathymetry data from *Ranero et al.* [2003].

changes from the 25 March earthquake to compare with the inland activity. The present study examines this sequence in more detail by computing static stress changes and those related to viscoelastic relaxation to understand the spatial and temporal stress variations associated with this sequence.

2. Seismicity Details

[8] The 25 March 1990 (UTC 1322:55.6) $M_w = 7.0$ earthquake occurred along the subduction megathrust at the Middle America Trench (Figure 1). In this location, the Cocos Plate subducts beneath the Caribbean Plate at ~8.5 cm/a, leading to large magnitude earthquakes on the subduction zone plate interface. This earthquake had a focal mechanism (strike of 292°, dip of 26°, and rake of 88° from *Protti et al.* [1995]) consistent with underthrusting at this subduction zone. On the basis of the approximate aftershock area of 1000 km^2 and seismic moment (M_o) of 1.1 × 10^{20} Nm, we estimate slip of 3 m averaged over this area. Details of the slip distribution suggest that it may have occurred in distinct patches related to a subducted seamount at depth [*Protti et al.*, 1995; *Bilek et al.*, 2003], although for our purposes here an average slip over the fault area will suffice. We also test a larger fault area of ~4000 km^2 as suggested by *Protti et al.* [1995] and correspondingly smaller fault slip (0.6 m) to explore how results will change on the basis of the chosen fault geometry.

[9] This earthquake produced a typical aftershock pattern of smaller events in the near-trench region that decayed in time following Omori's law (Figure 2). During the period between the main shock and 31 December, the seismic network operated by the OVSICORI (Observatorio Vulcanológico y Sismológico de Costa Rica) seismological group recorded thousands of aftershocks and cataloged the best located 4683 events (M. Protti and V. Gonzáles, personal communication, 2007) (Figure 1). Earthquakes were located using the HYPOINVERSE program with average horizontal location errors of 2.5 km and vertical errors of 5 km [*Protti et al.*, 1995]. These earthquakes range in local magnitude from 1.3 to 6.8 (main shock).

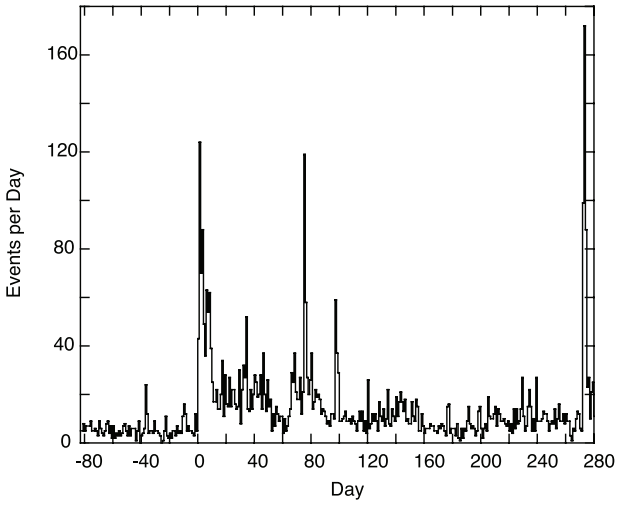

Figure 2. Seismicity through time in this region of Costa Rica (region of Figure 1). Day 0 is 25 March 1990 (main shock). Catalog extends from 1 January 1990 to 31 December 1990, with a total of 5151 events. Background level characterized by the pre–main shock date includes 468 events, whereas 4683 total earthquakes are contained in the post–main shock catalog. Large peak at day 75 (8 June) includes 119 events, the largest being a magnitude 4.5 in the inland region highlighted in Figure 1. Peak at day 273 (23 December) includes 172 events, preceded by a magnitude 5.7 event in the area on 22 December.

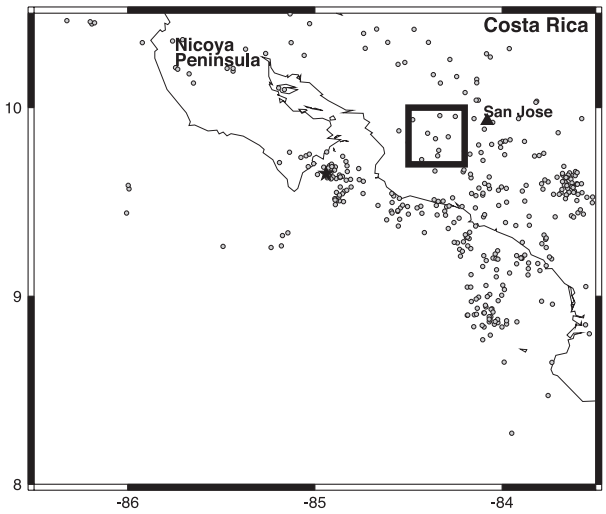

Figure 3. Map (same as Figure 1) showing seismicity during the period of 1 January 1990 to 24 March 1990. There was seismicity in the region of the 25 March main shock but very little activity (approximately 10 events) in the inland region of seismicity increase seen following the main shock (box).

[10] An anomalous sequence of earthquakes occurred inland of main shock slip region that did not behave as a typical aftershock sequence. This is also shown in Figure 2 as a large spike of activity occurred on 8 June, 75 days following the main shock and 23 December, 273 days following the main shock. In general, there is an increase in the activity rate from 65 to 90 days following the main shock, then reduces until 22 December when an M_w 5.7 event occurred within the inland region. This event leads to another spike of activity with 172 events occurring on 23 December (day 273 following the main shock). Earthquakes in the 60–90 day time period did not occur in the subduction zone megathrust region, but instead occurred in the inland region 75 km to the east of the main shock slip zone highlighted in Figure 1. This activity continued in the region throughout the rest of 1990. Note that this region was not previously very seismically active, as very few (less than 10) earthquakes occurred in this box during the 85 days prior to the main shock (Figure 3). During the 60–90 day period after the main shock, 493 events occurred within this cluster, which is also in the region of the mapped Holocene aged right-lateral strike-slip faults within the Picagres fault system [*Montero et al.*, 1998] (Figure 4). These events ranged in local magnitude from 1.7 to 4.5, with an average depth of 10 km (range from 0 to 49 km). During the 272–282 day period (22 December to 31 December), 426 events occurred in this region with a magnitude range of 1.8–5.7 and average depth of 12 km (0–85 km range).

3. Elastic Half-Space Calculations of Stress Change

[11] In order to examine the possibility of inland seismic triggering due to stress changes from the 1990 Nicoya event, we initially focus on stresses related to Coulomb failure. The change in Coulomb stress ($\Delta\sigma_f$) is related to a coefficient of friction (μ), change in pore pressure (Δp) and changes in shear ($\Delta\tau$) and normal ($\Delta\sigma_n$) stresses on the plane of failure by

$$\Delta\sigma_f = \Delta\tau + \mu(\Delta\sigma_n + \Delta p). \quad (1)$$

[12] For this study, we compute Coulomb stress changes due to slip in the 1990 Nicoya earthquake using the methods and Coulomb 3.1 software described by *Toda et al.* [2005]. These calculations use elastic dislocation formulae to compute stresses on receiver planes due to displacements within a half-space with uniform elastic properties [*Okada*,

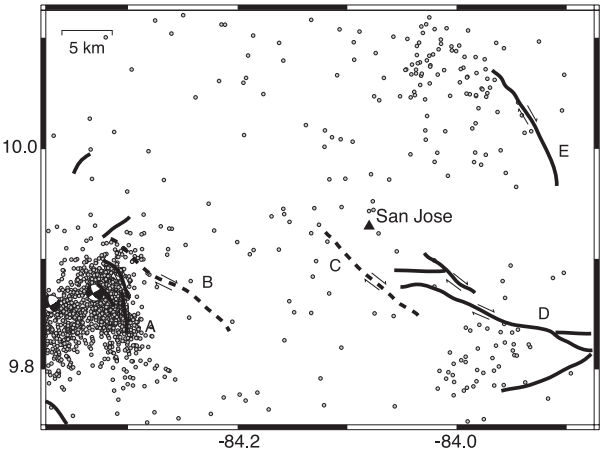

Figure 4. Post–main shock seismicity within the inland region of Figure 1 overlain with geologic map of the region, showing mapped Holocene (solid) or Quaternary (dashed) faults [*Montero et al.*, 1998]. Global CMT focal mechanisms plotted for the two largest aftershocks (30 June 1990 M_w 5.5 and 22 December 1990 M_w 5.9). Fault and fault groups are labeled as follows: A, Picagres fault system; B, Jaris Fault; C, Higuito Fault; D, Agua Caliente Fault; E, Lara Fault. Note that much of the seismicity clusters around the mapped group of right-lateral strike-slip faults in the Picagres system. We use the orientation of these faults (strike range from 325°–340°, dip of 90°, and rake of 180°) for the calculation of Coulomb stress change in this region.

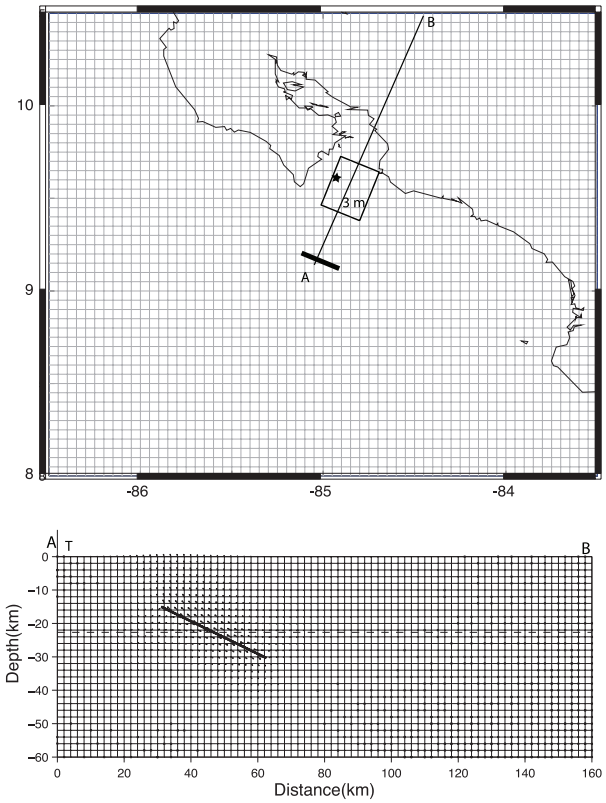

Figure 5. (top) Geometry used for Coulomb stress change calculations. Star indicates the 25 March 1990 epicenter, with surrounding box representing the area of slip (3 m of slip within the box). Fault geometry for this earthquake is strike of 292°, dip of 26°, and rake of 88°, consistent with underthrusting motion along the subducting plate interface. Trench position is shown by thick line. (bottom) A cross section through the model geometry, with the area of slip denoted by the bold solid line. Trench position is shown by T.

1992; *King et al.*, 1994; *Toda et al.*, 2005]. Inputs required are fault location, dip, model grid, Young's modulus (E), Poisson's ratio (ν), friction (μ), regional stress field, and amount of slip. Our model geometry is a reasonable approximation of the subduction fault and slip for this earthquake, using the trench location determined from bathymetry and a dip of 26° estimated from *Protti et al.* [1995] (Figure 5).

[13] The elastic parameters, E and ν, are constant throughout the model space, as this modeling technique does not allow for defining variable material properties in the slab, overriding plate, or along the plate boundary. Previous studies of fault displacement and corresponding stress changes have examined the results where E and ν vary within reasonable rock values and found only small changes in the stress change results [e.g., *Bilek and Lithgow-Bertelloni*, 2005]. Here we use reasonable values for the crustal rocks in this system, E of 8×10^4 MPa and ν of 0.25. The friction coefficient along the fault is defined between the range of 0–1. Previous studies have used values between 0.4 and 0.8, finding values near 0.4 more reasonable for subduction zone faulting [*Lin and Stein*, 2004]. Regions of strike-slip faulting as we find inland of the subduction fault may have higher friction, near 0.8 [*Lin and Stein*, 2004], so we test this value as well.

[14] Stress changes are calculated on receiver planes oriented to represent the mapped Holocene right-lateral strike-slip faults of the Picagres fault system. These faults range in strike between 325° and 340°, so we test fault orientations within this range. Without further knowledge about the fault orientations, we use a dip of 90° and a rake of 180°, reasonable values for a right-lateral strike-slip fault. We also calculate stress changes over a range of depths, from 5 to 15 km, bounding the region of most of the cluster event depths (average of 10–12 km).

[15] Values of Coulomb stress change computed on right-lateral strike-slip receiver planes of 340° strike show a multilobed pattern of increases and decreases (Figure 6). General comparisons with all of the aftershocks are not meaningful in this case, as many of the near-trench aftershocks are likely on the megathrust plane oriented differently than our receiver fault. Our focus is on the stress changes in the region of possible triggered events. Within this cluster of events, stress increases as large as 0.2 bars are observed (Figure 6) on receiver faults with a 340° strike. All of the inland events within this cluster fall within areas of stress increase, including those down to 30 km depth. Changing the strike of the receiver faults within the geologically observed range of 325°–340° affects the magnitude of the stress change. The maximum value in the region of interest using the other end-member strike of 325°, all other parameters fixed, is 0.4 bars. Stress changes computed on receiver faults oriented within this range vary between these two values.

[16] Within this model, we also find that the small increases in Coulomb stress observed at the inland locations are driven by changes in the normal stresses, effectively unclamping the receiver faults. Normal stress changes in the area of interest are 0.8 bars for 340° strike receiver faults and 0.7 bars on the 325° striking faults. This unclamping effect

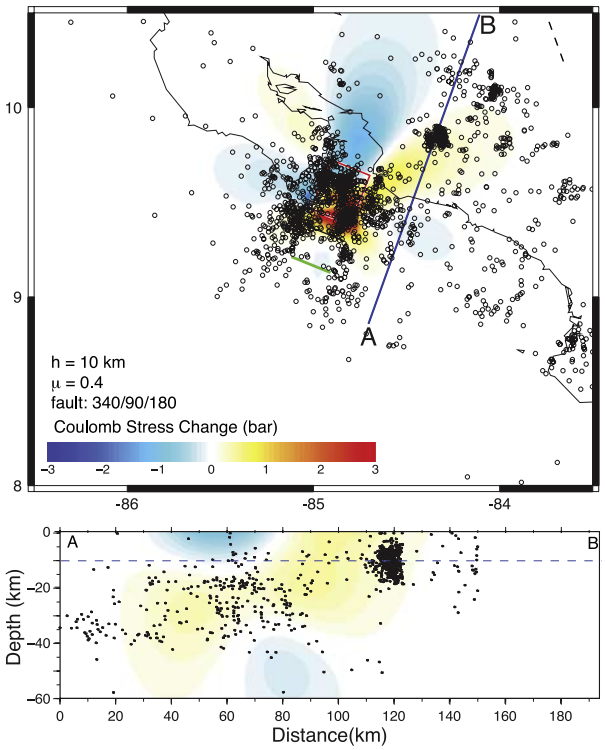

Figure 6. Coulomb stress changes as a result of slip along the subduction interface during the 25 March 1990 earthquake. (top) Stress changes (map view) are computed for receiver faults of orientation similar to the Picagres faults (strike 340°, dip 90°, and rake 180°), shown by dashed line in top right corner of map. Green line represents the trench location, red box indicates area of slip during earthquake, and circles are earthquakes occurring in the region within the 90 day period following the earthquake. Calculation depth shown here is 10 km, and coefficient of friction is 0.4. (bottom) Cross section through region of inland cluster. Stress changes here are less than 1 bar, with a maximum value in the inland cluster of 0.2 bars.

on fore-arc strike-slip faults has also been noted for faults in the northern Caribbean subduction system [*ten Brink and Lin*, 2004].

[17] Previous studies have suggested stress changes of over 0.5 bar in regions of triggered seismicity [*King et al.*, 1994], so this inland region falls below the triggering threshold based on the parameters described above. Thus we investigate how other model parameters may impact the stress changes in this region. First we modify the Young's modulus used to define the elastic properties of the entire model. Our initial (and preferred) model choice of 8×10^4 MPa has been used to examine stress changes in other subduction zones [*Lin and Stein*, 2004] and is also reasonable on the basis of the average crustal velocities used by *Protti et al.* [1995] for locating the earthquakes. Using higher average crustal velocities of V_p = 6.5 km/s in the back arc as determined by *Sallarès et al.* [2001] and *DeShon et al.* [2006] for portions of northern Costa Rica, the Young's modulus is larger at 1×10^5 MPa. Increasing the Young's modulus acts to increase the Coulomb stress change in the area of interest, and we find a maximum of 0.4 bar for a 340° strike receiver fault and 0.7 for a 325° strike fault. Stiffer material within the model allows for more effective transmission of stresses, thus producing the increases seen here.

[18] We also modify the coefficient of friction used for these faults. Because the faults of interest are relatively short strike-slip faults, a higher value of μ (0.8 instead of the original 0.4) might be more reasonable [e.g., *Lin and Stein*, 2004]. Using a μ = 0.8, we observe similar patterns to the result using μ = 0.4 (Figure 7). The magnitude of stress changes in the region of interest increases with

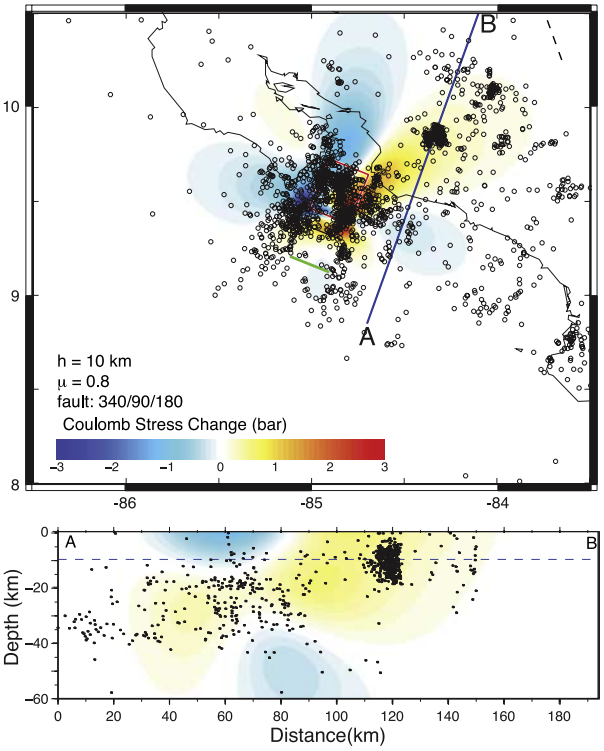

Figure 7. Coulomb stress changes as a result of slip along the subduction interface during the 25 March 1990 earthquake (same as Figure 6 but using a friction coefficient of 0.8). The pattern of stress change is similar to that for Figure 6, but the magnitude is slightly different. Stress changes in the cross section are also less than a bar, but the maximum value in the inland cluster region is approximately 0.5 bars.

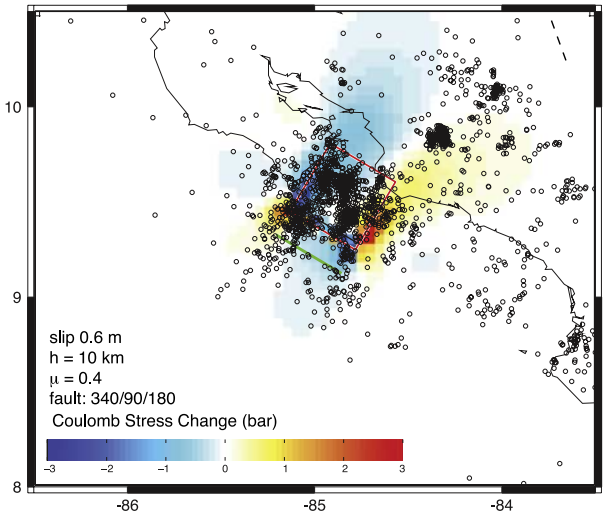

Figure 8. Coulomb stress changes as a result of 0.6 m of slip along an extended area along the subduction interface [*Protti et al.*, 1995]. Other parameters are the same as Figure 6. Magnitude of stress increases within the inland region range between 0.2 and 0.3 bars.

larger μ, as we calculate a maximum Coulomb stress change of 0.5 bar on 340° strike receiver faults and 0.8 bar at 325° strike. Finally, we modify the fault area and slip, using a lower estimate of slip (0.6 m) over a larger area as suggested by *Protti et al.* [1995] on the basis of the expansion of the aftershock pattern. We continue to see an increase in Coulomb stress in the inland region with magnitudes of 0.2–0.3 bars (Figure 8). Although there is less slip during the main shock, it occurred over a larger area that extends closer to the inland region of interest.

[19] Using the suite of model parameters described above, we find small increases that barely meet the commonly assumed minimum values for triggering. Thus it is possible that these events are simply triggered by the very small static stress increases from the 25 March event. However, because the 60–90 day delay before the peak of the first sequence, we also choose to examine one secondary triggering mechanism, that of viscoelastic relaxation, to see if this could also be a factor in the delayed triggering of these events.

4. Finite Element Modeling With Variable Material Parameters

[20] The viscoelastic response of the subduction zone system acts to modify stresses in the system over a period of time and cannot be addressed in the purely elastic model parameterization described in the previous section. Thus we use a commercially available finite element program (ABAQUS) that provides the freedom to generate realistic model geometry as well as model material properties relevant for a subduction zone system. This type of model has been used effectively to model faults with multiple layered rheology and in subduction zone settings [e.g., *Taylor et al.*, 1998; *Kenner and Segall*, 1999; *Masterlark et al.*, 2001; *Masterlark*, 2003].

[21] Because of the geometric complexity, this paper provides only a 2-D representation of slip in a subduction zone, modeled after the geometry of central Costa Rica in plate thickness and dip angle. Because of the differences in parameterization of the slip, geometry, and boundary conditions, results here will not be useful for direct comparison with the Coulomb results. Our goal here is to look at general features relevant to our region of interest. Specifically, is there an area ~100 km from the trench that shows an increase in stress in response to slip from a M 7 earthquake on the boundary within the time period of interest?

[22] The 2-D model geometry is similar to that generated in the previous case, but we have added

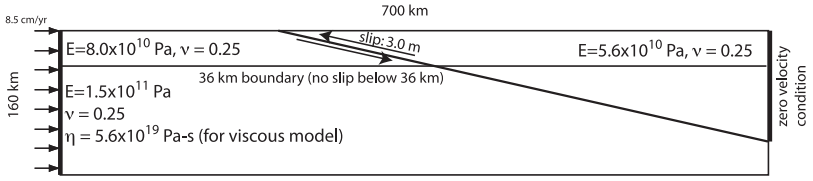

Figure 9. Schematic of the FEM used for the Costa Rica geometry. Slip of 3 m is applied along the upper plate boundary. A velocity of 8.5 cm/a is applied on the left edge of the model to represent average convergence rate at this region. The top right edge of the model is held fixed by a zero velocity boundary condition to mimic the overriding plate backstop. Upper oceanic crustal material (from 0 to 36 km) is defined by a Young's modulus (E) of 8.0×10^{10} Pa and Poisson's ratio (ν) of 0.25. We use a reasonable value of E = 5.6×10^{10} Pa for continental crust. We use an E of 1.1×10^{11} Pa and ν of 0.25 for the mantle material down to 160 km. For these viscoelastic simulations, a viscosity ($\eta = 5.6 \times 10^{19}$ Pa s) is applied to the mantle material to produce the viscoelastic behavior for the mantle.

additional layers to mimic the subducting slab and overriding plate (Figure 9). The model dimensions are 700 km perpendicular to the trench and 160 km in depth extent to reduce problems with edge effects within the model. Individual components of the model are parameterized with material properties appropriate for continental crust, subducting oceanic crust, and mantle (Table 1). There is a boundary at 40 km depth in the model indicating the transition from crust to mantle. This boundary depth is reasonable on the basis of crustal thickness results of 36–40 km using receiver functions in this region (stations LSOL and ZAPA, [*MacKenzie et al.*, 2008]) as well as regional estimates of the continental Moho from 3-D velocity models of *DeShon et al.* [2006]. We also tested the effect of reducing the crustal thickness to 27 km, which is the shallowest Moho depth found by *MacKenzie et al.* [2008] within central Nicoya Peninsula and changing the dip to reflect an increase at the downdip edge.

[23] Slip and boundary conditions are applied along the dipping boundary and the sides of the box. Slip of 3 m, reasonable for the displacement of this earthquake, is applied using a tangential (or relative) sliding between the upper and lower plates along the dipping boundary from the surface to the downdip crustal boundary. A friction coefficient of 0.4 is applied along the dipping boundary. A zero velocity condition is applied along the upper right edge of the model containing the upper plate, thus holding this portion of the model fixed. This is a reasonable condition for our subduction zone geometry, with the margin wedge held fixed against a landward backstop. A velocity of 8.5 cm/a was applied on the entire left edge of the model to represent the convergence of the subducting Cocos Plate at the trench.

[24] We parameterize a viscoelastic mantle using the finite element model (FEM) to allow for relaxation in the mantle following the slip at time = 0. This was achieved by adding a power law creep component to the layer below 40 km using the FEM defined creep material options. The creep model is defined as

$$\overline{\varepsilon} = (Aq^n[(m+1)\overline{\varepsilon}^{cr}]^m)^{\frac{1}{(m+1)}} \quad (2)$$

where $\overline{\varepsilon}$ is the uniaxial equivalent strain rate, $\overline{\varepsilon}^{cr}$ is the uniaxial equivalent creep rate, q is the uniaxial equivalent deviatoric stress, and A, m, and n are user defined quantities dependent on viscosity, time, and strain respectively. Here we use n = 1 and m = 0 for the exponents for strain and time, making this relationship linear, and mimicking a Newtonian solid. Viscosity and other elastic parameters used for this model are given in Table 1. The mantle viscosity used here (5.6×10^{19} Pa s) is consistent with values used to examine postseismic relaxation in Japan (6×10^{19} Pa s [*Pollitz et al.*, 2006]), and following the 2004 Sumatra earthquake (10^{19} Pa s [*Pollitz et al.*, 2008]). With this model, we compute stresses for 14 increasing time steps from 1 s following the applied slip, to 120 days in 15 day increments to cover the time period of increased seismicity, to 4 years with much larger time increments to explore the longer-period behavior of the model. Because our goal here is only to probe whether stresses within the inland area could be affected by the viscoelastic relaxation and not a direct comparison with the Coulomb stress change results presented above, we show the von Mises stress magnitudes as a measure of the deviatoric stress (Figure 10).

Table 1. FEM Material Parameters

Material	Young's Modulus (Pa)	ν	η (Pa s)
Continental crust	5.6×10^{10}	0.25	
Oceanic crust	8.0×10^{10}	0.25	
Mantle	1.1×10^{11}	0.25	5.6×10^{19}

[25] Maximum stress occurs in the first 1 s time step in a small region at the top of the mantle material beneath the overriding crust within the model. The peak stress at each subsequent time period decreases from the 1 s value and remains concentrated at the crust-mantle boundary between the dipping interface. However, more relevant to the problem here are stresses within the inland region of high seismicity levels (box in Figure 10). Within the first several time steps out to 15 days following the applied slip, stresses within the inland region are small at a few MPa, not above the background level of the model (Figures 10a–10c). At the 30 day time step, stresses increase above the background level in this region to above 100 MPa (Figure 10d). Stress levels within the inland region remain high (above 230 MPa) through the 150 day time step (Figure 10h). Following this time step, the inland stress values decrease through the 4 year time step (Figures 10i–10n). The pattern of stress increase and decrease reflects the finite time scale for the propagation of the viscous stresses within the mantle and is consistent with the seismicity increase between 60 and 90 days. Again we note that the

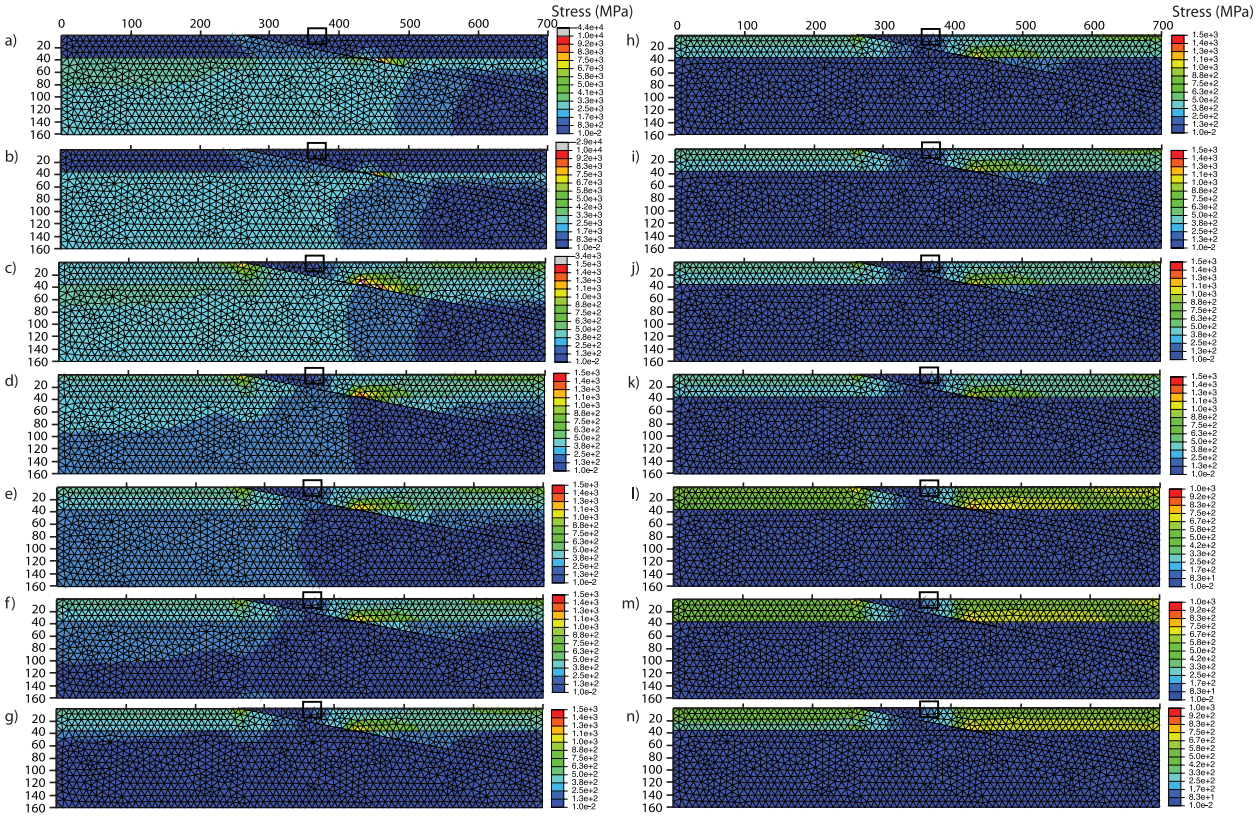

Figure 10. Stress changes within the viscoelastic 2-D model due to displacement along the interface. T indicates the trench position, and the black box outlines the area of the inland seismicity cluster. von Mises stresses (combination of σ_1 and σ_2) are plotted (color bar) for the elements in the model for 14 time steps: (a) 1s, (b) 1 day, (c) 15 days, (d) 30 days, (e) 45 days, (f) 60 days, (g) 75 days, (h) 90 days, (i) 105 days, (j) 120 days, (k) 150 days, (l) 300 days, (m) 2 years, and (n) 4 years. Early time steps show very little stress within the inland region; however, by 30 days, there is an increase in stress within this area by 130–230 MPa. At the 300 day time step, stresses in this region drop below 100 MPa and continue to decrease in value through the 4 year time step (Figure 10n). Peak stresses appear at the prescribed boundaries between model components, such as at the continental crust, slab, and mantle boundary (~450 km from the edge of model).

exact values of the stress are less important here than the qualitative observation of an increase in this region due to the incorporation of the viscoelastic mantle.

[26] We tested a range of dynamic viscosities between 2 orders of magnitude from our original value of 5×10^{19} Pa s. Because we hold the velocities constant, the effect of the change in viscosity is to change the magnitude of the stresses, but not the overall spatial distribution. Stress increases were larger for lower viscosities and smaller at larger viscosities as expected for a linear rheology. In addition, the time scale of the stress changes is affected by the viscosity differences, with more rapid transmission of stress changes for the lower-viscosity mantle and longer time to observe changes for the more viscous mantle. We also reduced the crustal thickness to 27 km, finding similar magnitudes of stress, but the entire pattern shifts trenchward because the slab/mantle boundary is shallower, bringing larger stresses into the region of inland seismicity. Similarly, we increased the dip of the slab between 26 and 45° [e.g., *Norabuena et al.*, 2004] and again we see the increases stresses move trenchward, increasing the stress magnitudes in the inland seismicity region.

[27] Clearly a 3-D model including realistic rheologic parameters is desired to more completely understand the role of the viscoelastic relaxation on this delayed seismicity; this however is beyond the scope of this paper. The 2-D model does show an increase in stress within the time scales of interest however, larger than we see for the coseismic increases only. This result allows us to suggest

that viscoelastic relaxation is a possible mechanism for the delayed triggering of these events.

[28] *Taylor et al.* [1998] examined stresses within the upper plate following large earthquakes in oblique subduction zones such as the Aleutians. Using a 3-D FEM, they computed Coulomb stresses resulting from oblique slip along a portion of the megathrust, finding zones of upper plate stress increases in the areas where subsequent large earthquakes occurred within days to years. They focused primarily on the larger events in oblique zones, but we find similar results for the Costa Rica margin with less oblique convergence.

5. Discussion

[29] The inland seismicity that increased in 2 distinct time periods, 60–90 days and 270 days, following the 25 March 1990 subduction zone event had previously been suggested as triggered events [*Protti et al.*, 1995]. Results from stress change modeling using purely elastic material parameters show small increases of up to 0.8 bars, depending on the elastic parameters and coefficient of friction. The time delay is another interesting aspect of this earthquake sequence, leading to a possible delayed triggering mechanism of visco-elastic relaxation of the mantle beneath the fault zone.

[30] Other possibilities exist for delayed triggering, and we review these below. Poroelastic effects as well as more complex friction parameterization, such as rate- and state-dependent friction, might be important for triggering here as has been suggested for other areas, but we do not explore these parameterizations here. We do not suspect dynamic triggering of these events by the passage of surface waves following the 25 March event as the time delay is much longer (weeks to months) than the minutes to hours expected for dynamic triggering from the main shock. Additionally, there was no large magnitude event during this time period that has characteristics (appropriate distance, directivity effects) required to cause dynamic triggering of these events.

[31] It appears that not all large magnitude earthquakes along this margin produce time delayed triggering. The 20 August 1999 M_w = 6.9 Quepos earthquake had a typical aftershock pattern with no noticeable inland clusters, although there are no mapped strike-slip faults inland of this region [*Montero et al.*, 1998].

[32] This study also suggests a need to examine the inland seismic hazard within Costa Rica. Much effort has been placed on defining past earthquakes and recurrence on the subduction megathrust at the Middle America Trench. However, there are many strike-slip faults inland of this section of the subduction zone. On the basis of the regional stress field for this region as estimated from the World Stress Map [*Heidbach et al.*, 2004], and slip on the megathrust oriented at 290° strike, the optimally oriented right-lateral strike-slip faults within this inland region strike at approximately 345°, similar to the 325–340° strike of the Picagres system examined here. It is also similar to the 310–335° strike orientation of the Higuito and Lara faults (Figure 4). The cluster of earthquakes triggered here were generally small magnitude (less than M 4.5) and appear to be located on relatively short segments (<5 km long) in the Picagres fault system (Figure 4). However, there are longer (15–20 km) mapped fault segments, such as the Jaris, Higuito, and Lara fault systems, which are also roughly optimally oriented, that are located within 20 km of San Jose, Costa Rica. The population of San Jose and the surrounding Central Valley reaches over 2 million.

[33] Interestingly, *ten Brink and Lin* [2004] argued that stress changes resulting from repeated large earthquakes can influence the deformation of the fore arc, specifically the orientations of optimally oriented strike-slip faults. In both general models as well as specific cases in the northern Caribbean subduction zone, they found earthquake ruptures with small slip angles relative to the convergence direction tend to influence strike-slip faults further from the trench. This connection between large earthquake ruptures and regional strike-slip faults is similar to our results for the Costa Rica case. Repeated $M \sim 7$ subduction zone earthquakes offshore this portion of central Costa Rica may be linked to the orientation of the inland strike-slip faults.

[34] We show here that triggered seismicity is certainly possible on these inland faults following a large subduction zone earthquake in the Nicoya Gulf region of the Middle America Trench. *Protti et al.* [1995] estimated a recurrence time of 50 years for events in the Nicoya Gulf region. Because the 25 March 1990 earthquake was likely the result of rupture of a subducted seamount contact with the overriding Caribbean Plate [*Protti et al.*, 1995; *Husen et al.*, 2002; *Bilek et al.*, 2003], the rupture area and magnitude of the earthquakes in this

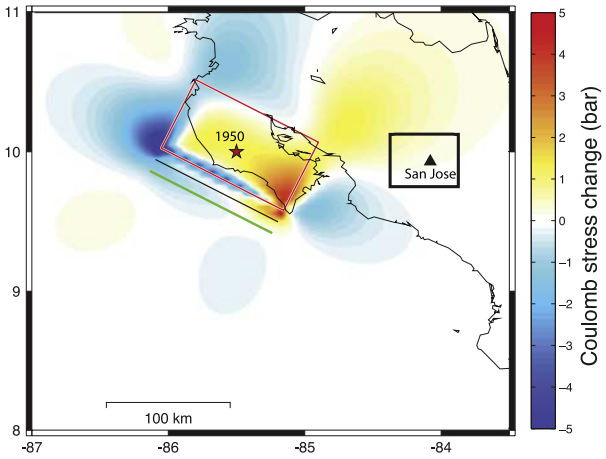

Figure 11. Coulomb stress change estimates as a result of a 1950-type M_w = 7.7 earthquake on the subduction thrust. Epicenter of the 1950 earthquake (star [*Protti et al.*, 1995]) and estimated rupture area (red box [*Avants et al.*, 2001]) are used to compute stress changes. Subduction zone geometry is estimated from *DeShon et al.* [2006]. Stress changes are computed on right-lateral strike-slip receiver faults oriented with a 340° strike for comparison with Figure 6. Friction coefficient is 0.4. Triangle shows location of San Jose, and the black box outlines region of strike-slip faulting in Figure 4. Maximum stress changes at 10 km within this box are 0.6 bars, with values between 0.4 and 0.6 bars computed on receiver faults with a range of mapped orientations of 310°–340°. Increased μ for these faults increases the stress change values in the box, similar to that seen in Figure 7.

segment are likely limited to the $M \sim 7$ range. Thus the stress changes and implications for inland triggering shown here are reasonable estimates for future Nicoya earthquakes and other central Costa Rica earthquakes where other seamounts subduct and influence earthquake rupture.

[35] However, the Nicoya Peninsula region, north of the Nicoya Gulf, has ruptured in earthquakes of $M > 7.5$ [*Protti et al.*, 1994]. Rupture estimates for the $M_w = 7.7$ 1950 underthrusting earthquake cover much of the Nicoya Peninsula [*Güendel*, 1986; *Avants et al.*, 2001]. On the basis of the historical catalog, *Nishenko* [1989] listed this region as a significant seismic gap. In the Nicoya Peninsula region, Cocos crust originating from the East Pacific Rise is much smoother than the seamount-dominated crust that originated at the Cocos Nazca spreading center and subducts beneath central Costa Rica. The smoother crust may allow for stronger plate coupling and larger earthquakes in the Nicoya Peninsula region than in central Costa Rica [*Protti et al.*, 1994, 1995]. *Norabuena et al.* [2004] inverted GPS velocities measured along the Nicoya Peninsula to find a patch of strongly coupled plate interface in the shallow portion of the megathrust. Thus an $M > 7.5$ earthquake is quite possible along this portion of the margin. Using the rupture area and size of the 1950 earthquake, we compute possible Coulomb stress changes due to the 1950 earthquake along faults to the southwest of San Jose. Our results suggest increases of 0.4 bars in the area and orientation of the Higuito fault, 0.5 bars in the area of the Jaris fault, and 0.6 bars on the faults in the Picagres system (Figure 11). Because of the longer length of the Higuito and Jaris faults relative to the Picagres system, triggered events on these faults might be larger magnitude and of more concern for hazard assessments of the capital region.

6. Conclusions

[36] The 1990 Nicoya earthquake along the central coast of Costa Rica produced a typical aftershock sequence of earthquakes likely on the subduction megathrust zone as well as a secondary set of earthquakes between 60 and 90 days and 270 days following the main shock 75 km inland from the slip zone. We suggest that these events were triggered by the 1990 main shock, through either minor increases in Coulomb stress within the region or in combination with viscoelastic relaxation of the underlying mantle. Coulomb stress increases along mapped right-lateral strike-slip faults in this region tend to be small (<1 bar), but very close to accepted triggering thresholds. Stresses arising between 30 and 150 days following the slip within a viscoelastic FEM also increase inland of the rupture zone. Thus a combination of these stresses is a plausible explanation for both the spatial and temporal seismicity patterns observed after this earthquake. Because of other optimally oriented strike-slip faults mapped inland of the trench, we suggest that hazard assessments for the San Jose region include possible triggering from megathrust events 100 km away at the Middle America Trench.

Acknowledgments

[37] We gratefully acknowledge comments from the reviewers (Marino Protti and Heather DeShon) and the Associate Editor that strengthened the paper. Support for this work has been provided by the NSF Geophysics program grant EAR-0440243 to S.L.B. and EAR-0440229 to C.L.B. Seismic data were provided by M. Protti and V. Gonzáles of OVSICORI.

References

Anderson, G., and H. Johnson (1999), A new statistical test for static stress triggering: Application to the 1987 Superstition Hills earthquake sequence, *J. Geophys. Res.*, *104*, 20,153–20,168, doi:10.1029/1999JB900200.

Avants, M., S. Y. Schwartz, A. V. Newman, and H. R. DeShon (2001), Large underthrusting earthquakes beneath the Nicoya Peninsula, *Eos Trans. AGU*, *82*(47), Fall Meet. Suppl., Abstract T52E-07.

Bilek, S. L., and C. Lithgow-Bertelloni (2005), Stress changes in the Costa Rica subduction zone due to the 1999 Mw = 6.9 Quepos earthquake, *Earth Planet. Sci. Lett.*, *230*, 97–112, doi:10.1016/j.epsl.2004.11.020.

Bilek, S. L., S. Y. Schwartz, and H. R. DeShon (2003), Control of seafloor roughness on earthquake rupture behavior, *Geology*, *31*, 455–458, doi:10.1130/0091-7613(2003)031<0455:COSROE>2.0.CO;2.

Brodsky, E. E., and S. G. Prejean (2005), New constraints on mechanisms of remotely triggered seismicity at Long Valley Caldera, *J. Geophys. Res.*, *110*, B04302, doi:10.1029/2004JB003211.

Brodsky, E. E., E. Roeloffs, D. Woodcock, I. Gall, and M. Manga (2003), A mechanism for sustained groundwater pressure changes induced by distant earthquakes, *J. Geophys. Res.*, *108*(B8), 2390, doi:10.1029/2002JB002321.

Cotton, F., and O. Coutant (1997), Dynamic stress variations due to shear faults in a plane-layered medium, *Geophys. J. Int.*, *128*, 676–688, doi:10.1111/j.1365-246X.1997.tb05328.x.

DeShon, H. R., S. Y. Schwartz, A. V. Newman, V. Gonzáles, M. Protti, L. M. Dorman, T. H. Dixon, D. E. Simpson, and E. R. Flueh (2006), Seismogenic zone structure beneath the Nicoya Peninsula, Costa Rica, from three-dimensional local earthquake P- and S-wave tomography, *Geophys. J. Int.*, *164*, 109–124, doi:10.1111/j.1365-246X.2005.02809.x.

Dreger, D. S., and A. Kaverina (2000), Seismic remote sensing for the earthquake source process and near-source strong shaking: A case study of the October 16, 1999 Hector Mine earthquake, *Geophys. Res. Lett.*, *27*, 1941–1944, doi:10.1029/1999GL011245.

Freed, A. M. (2005), Earthquake triggering by static, dynamic, and postseismic stress transfer, *Annu. Rev. Earth Planet. Sci.*, *33*, 335–367, doi:10.1146/annurev.earth.33.092203.122505.

Freed, A. M., and J. Lin (1998), Time-dependent changes in failure stress following thrust earthquakes, *J. Geophys. Res.*, *103*, 24,393–24,409, doi:10.1029/98JB01764.

Gomberg, J., P. Bodin, K. Larson, and H. Dragert (2004), Earthquake nucleation by transient deformations caused by the *M* = 7.9 Denali, Alaska, earthquake, *Nature*, *427*, 621–624, doi:10.1038/nature02335.

Güendel, F. (1986), Seismotectonics of Costa Rica: An analytical view of the southern terminus of the Middle America Trench, Ph.D. dissertation, 157 pp., Univ. of Calif., Santa Cruz.

Hardebeck, J. L., J. J. Nazareth, and E. Hauksson (1998), The static stress change triggering model: Constraints from two southern California aftershock sequences, *J. Geophys. Res.*, *103*, 24,427–24,437, doi:10.1029/98JB00573.

Hauksson, E., L. M. Jones, K. Hutton, and D. Eberhart-Phillips (1993), The 1992 Landers earthquake sequence: Seismological observations, *J. Geophys. Res.*, *98*, 19,835–19,858, doi:10.1029/93JB02384.

Heidbach, O., A. Barth, P. Connolly, K. Fuchs, B. Müller, J. Reinecker, B. Sperner, M. Tingay, and F. Wenzel (2004), Stress maps in a minute: The 2004 World Stress Map release, *Eos Trans. AGU*, *85*(49), 521–529, doi:10.1029/2004EO490001.

Hill, D. P., P. A. Reasenberg, A. J. Michael, W. J. Arabasz, and G. C. Beroza (1993), Seismicity remotely triggered by the magnitude 7.3 Landers, California earthquake, *Science*, *260*, 1617–1623, doi:10.1126/science.260.5114.1617.

Husen, S., E. Kissling, and R. Quintero (2002), Tomographic evidence for a subducted seamount beneath the Gulf of Nicoya, Costa Rica: The cause of the 1990 Mw = 7.0 Gulf of Nicoya earthquake, *Geophys. Res. Lett.*, *29*(8), 1238, doi:10.1029/2001GL014045.

Kenner, S., and P. Segall (1999), Time-dependence of the stress shadowing effect and its relation to the structure of the lower crust, *Geology*, *27*, 119–122, doi:10.1130/0091-7613(1999)027<0119:TDOTSS>2.3.CO;2.

King, G. C. P., R. S. Stein, and J. Lin (1994), Static stress changes and the triggering of earthquakes, *Bull. Seismol. Soc. Am.*, *84*, 935–993.

Lin, J., and R. S. Stein (2004), Stress triggering in thrust and subduction earthquakes, and stress interaction between the southern San Andreas and nearby thrust and strike-slip faults, *J. Geophys. Res.*, *109*, B02303, doi:10.1029/2003JB002607.

MacKenzie, L., G. A. Abers, K. M. Fischer, E. M. Syracuse, J. M. Protti, V. Gonzales, and W. Strauch (2008), Crustal structure along the southern Central American volcanic front, *Geochem. Geophys. Geosyst.*, *9*, Q08S09, doi:10.1029/2008GC001991.

Masterlark, T. (2003), Finite element model predictions of static deformation from dislocation sources in a subduction zone: Sensitivities to homogeneous, isotropic, Poisson-solid, and half-space assumptions, *J. Geophys. Res.*, *108*(B11), 2540, doi:10.1029/2002JB002296.

Masterlark, T., C. DeMets, H. F. Wang, O. Sanchez, and J. Stock (2001), Homogeneous vs heterogeneous subduction zone models: Coseismic and postseismic deformation, *Geophys. Res. Lett.*, *28*, 4047–4050, doi:10.1029/2001GL013612.

Montero, W., P. Denyer, R. Barquero, G. Alvarado, and H. Cowan (1998), Map of quaternary faults and folds of Costa Rica, *U.S. Geol. Surv. Open File Rep., 98-0481*.

Nishenko, S. P. (1989), Circumpacific seismic potential 1989–1999, *U.S. Geol. Surv. Open File Rep., 89-86*.

Norabuena, E., et al. (2004), Geodetic and seismic constraints on some seismogenic zone processes in Costa Rica, *J. Geophys. Res.*, *109*, B11403, doi:10.1029/2003JB002931.

Okada, Y. (1992), Internal deformation due to shear and tensile faults in a half space, *Bull. Seismol. Soc. Am.*, *83*, 1018–1040.

Parsons, T. (2005), A hypothesis for delayed dynamic triggering, *Geophys. Res. Lett.*, *32*, L04302, doi:10.1029/2004GL021811.

Pollitz, F. F., and S. I. Sacks (2002), Stress triggering of the 1999 Hector Mine earthquake by transient deformation following the 1992 Landers earthquake, *Bull. Seismol. Soc. Am.*, *92*, 1487–1496, doi:10.1785/0120000918.

Pollitz, F. F., M. Nyst, T. Nishimura, and W. Thatcher (2006), Inference of postseismic deformation mechanisms of the 1923 Kanto earthquake, *J. Geophys. Res.*, *111*, B05408, doi:10.1029/2005JB003901.

Pollitz, F., P. Banerjee, K. Grijalva, B. Nagarajan, and R. Bürgmann (2008), Effect of 3-D viscoelastic structure on post-seismic relaxation from the 2004 *M* = 9.2 Sumatra earthquake, *Geophys. J. Int.*, *173*, 189–204, doi:10.1111/j.1365-246X.2007.03666.x.

Protti, M., F. Güendel, and K. McNally (1994), The geometry of the Wadati-Benioff zone under southern Central America and its tectonic significance: Results from a high-resolution local seismographic network, *Phys. Earth Planet. Inter.*, *84*, 271–287, doi:10.1016/0031-9201(94)90046-9.

Protti, M., et al. (1995), The March 25, 1990 (M_w = 7.0, M_L = 6.8), earthquake at the entrance of the Nicoya Gulf, Costa Rica: Its prior activity, foreshocks, aftershocks, and triggered seismicity, *J. Geophys. Res.*, *100*, 20,345–20,358, doi:10.1029/94JB03099.

Ranero, C. R., J. P. Morgan, K. McIntosh, and C. Reichert (2003), Bending-related faulting and mantle serpentinization at the Middle America Trench, *Nature*, *425*, 367–373, doi:10.1038/nature01961.

Reasenberg, P. A., and R. W. Simpson (1992), Response of regional seismicity to the static stress change produced by the Loma Prieta earthquake, *Science*, *255*, 1687–1690, doi:10.1126/science.255.5052.1687.

Roeloffs, E., M. Sneed, D. L. Galloway, M. L. Sorey, C. D. Farrar, J. F. Howle, and J. Hughes (2003), Water-level changes induced by local and distant earthquakes at Long Valley caldera, California, *J. Volcanol. Geotherm. Res.*, *127*, 269–303, doi:10.1016/S0377-0273(03)00173-2.

Sallarès, V., J. J. Dañobeitia, and E. R. Flueh (2001), Lithospheric structure of the Costa Rican Isthmus: Effects of subduction zone magmatism on an oceanic plateau, *J. Geophys. Res.*, *106*, 621–643, doi:10.1029/2000JB900245.

Steacy, S., D. Marson, S. S. Nalbant, and J. McCloskey (2004), Sensitivity of static stress calculations to the earthquake slip distribution, *J. Geophys. Res.*, *109*, B04303, doi:10.1029/2002JB002365.

Stein, R. S. (1999), The role of stress transfer in earthquake occurrence, *Nature*, *402*, 605–609, doi:10.1038/45144.

Taylor, M. A. J., R. Dmowska, and J. R. Rice (1998), Upper plate stressing and seismicity in the subduction earthquake cycle, *J. Geophys. Res.*, *103*, 24,523–24,542, doi:10.1029/98JB00755.

ten Brink, U., and J. Lin (2004), Stress interaction between subduction earthquakes and forearc strike-slip faults: Modeling and application to the northern Caribbean plate boundary, *J. Geophys. Res.*, *109*, B12310, doi:10.1029/2004JB003031.

Toda, S., R. S. Stein, P. A. Reasenberg, J. H. Dieterich, and A. Yoshida (1998), Stress transferred by the 1995 Mw = 6.9 Kobe, Japan, shock: Effect on aftershocks and future earthquake probabilities, *J. Geophys. Res.*, *103*, 24,543–24,565, doi:10.1029/98JB00765.

Toda, S., R. S. Stein, K. Richards-Dinger, and S. Bozkurt (2005), Forecasting the evolution of seismicity in southern California: Animations built on earthquake stress transfer, *J. Geophys. Res.*, *110*, B05S16, doi:10.1029/2004JB003415.

Velasco, A. A., S. Hernandez, T. Parsons, and K. Pankow (2008), Global ubiquity of dynamic earthquake triggering, *Nat. Geosci.*, *1*, 375–379, doi:10.1038/ngeo204.